5-2-2014

Very Low Frequency Subionospheric Remote Sensing of Thunderstorm-Driven Acoustic Waves in the Lower Ionosphere

R. A. Marshall
Stanford University

J. B. Snively
Embry-Riddle Aeronautical University, snivelyj@erau.edu

AGU PUBLICATIONS

JGR

Journal of Geophysical Research: Atmospheres

RESEARCH ARTICLE

10.1002/2014JD021594

Key Points:
- We report observations of acoustic waves in the *D* region using VLF remote sensing
- We model the acoustic wave and VLF transmitter signal to reproduce the event
- A very large source is required to reproduce the amplitude in the VLF data

Correspondence to:
R. A. Marshall,
ram80@stanford.edu

Citation:
Marshall, R. A., and J. B. Snively (2014), Very low frequency subionospheric remote sensing of thunderstorm-driven acoustic waves in the lower ionosphere, *J. Geophys. Res. Atmos.*, *119*, 5037–5045, doi:10.1002/2014JD021594.

Received 30 JAN 2014
Accepted 7 APR 2014
Accepted article online 13 APR 2014
Published online 2 MAY 2014

Very low frequency subionospheric remote sensing of thunderstorm-driven acoustic waves in the lower ionosphere

R. A. Marshall[1] and J. B. Snively[2]

[1]Department of Aeronautics and Astronautics, Stanford University, Stanford, California, USA, [2]Department of Physical Sciences, Embry-Riddle Aeronautical University, Daytona Beach, Florida, USA

Abstract We present observations of narrowband subionospheric VLF transmitter signals on 20 March 2001, exhibiting coherent fluctuations of over 1 dB peak to peak. Spectral analysis shows that the fluctuations have periods of 1–4 min and are largely coherent. The subionospheric propagation path of the signal from Puerto Rico to Colorado passes over two regions of convective and lightning activity, as observed by GOES satellite imagery and National Lightning Detection Network lightning data. We suggest that these fluctuations are evidence of acoustic waves launched by the convective activity below, observed in the 80–90 km altitude range to which nighttime VLF subionospheric remote sensing is sensitive. These observations show that VLF subionospheric remote sensing may provide a unique, 24 h remote sensing technique for acoustic and gravity wave activity. We reproduce this event in simulations using a fluid model of gravity and acoustic wave propagation to calculate the ionospheric disturbance, followed by an electromagnetic propagation model to calculate the perturbation amplitude at the location of the VLF receiver. Simulation results show that a very large and coherent convective source is required to produce these amplitude perturbations.

1. Introduction

Convectively generated gravity waves (GWs) are routinely observed in the mesosphere and ionosphere; they influence atmospheric circulation, structure, and variability at mesospheric and thermospheric altitudes [e.g., *Fritts and Alexander*, 2003, and references therein]. Lesser known are the effects of acoustic waves on the upper atmosphere [e.g., *Laštovička*, 2006]. Significant evidence exists for atmospheric waves of 1–5 min periods in the *F* region ionosphere associated with severe weather in the troposphere [*Georges*, 1973, and references therein]. Waves with frequencies above the Brunt-Väisälä frequency have also been observed in airglow image [*Hecht et al.*, 2002] and spectral data [*Pilger et al.*, 2013]. Acoustic and gravity waves were also observed in the *F* region ionosphere following the 2011 Tohoku, Japan, earthquake and tsunami as modifications to the ionospheric electron density [e.g., *Matsumura et al.*, 2011; *Galvan et al.*, 2012, and references therein]; in situ satellite measurements detected acoustic waves in the *F* region with periods of ~1 min that perturbed the neutral density by up to ~11% [*Garcia et al.*, 2013].

Acoustic waves are not easily observed in airglow imager data, due to relatively weak airglow perturbations except directly above sources and the need for imaging cadences of less than a minute [*Snively*, 2013]. In this paper, we present observations of acoustic waves propagating through the *D* region ionosphere using VLF subionospheric remote sensing (VLF-SRS). This technique is extremely sensitive to fluctuations in the *D* region electron density in a narrow altitude range near 85 km (the VLF reflection height). This method provides a 24 h, weatherproof, high-time-resolution detection method for acoustic and gravity waves propagating through the *D* region. It appears most sensitive to acoustic waves that produce horizontally coherent perturbations over the VLF wave propagation paths between transmitters and receivers.

2. Observations

Stanford has operated the Holographic Array for Ionosphere and Lightning Research (HAIL) since the late 1990s, primarily to study the effects of lightning on the *D* region ionosphere [e.g., *Johnson et al.*, 1999; *Peter and Inan*, 2005; *Marshall et al.*, 2006]. Each VLF receiver consists of orthogonal magnetic loop antennas, which are fed into a low-noise preamplifier. The signals are then filtered and amplified again before

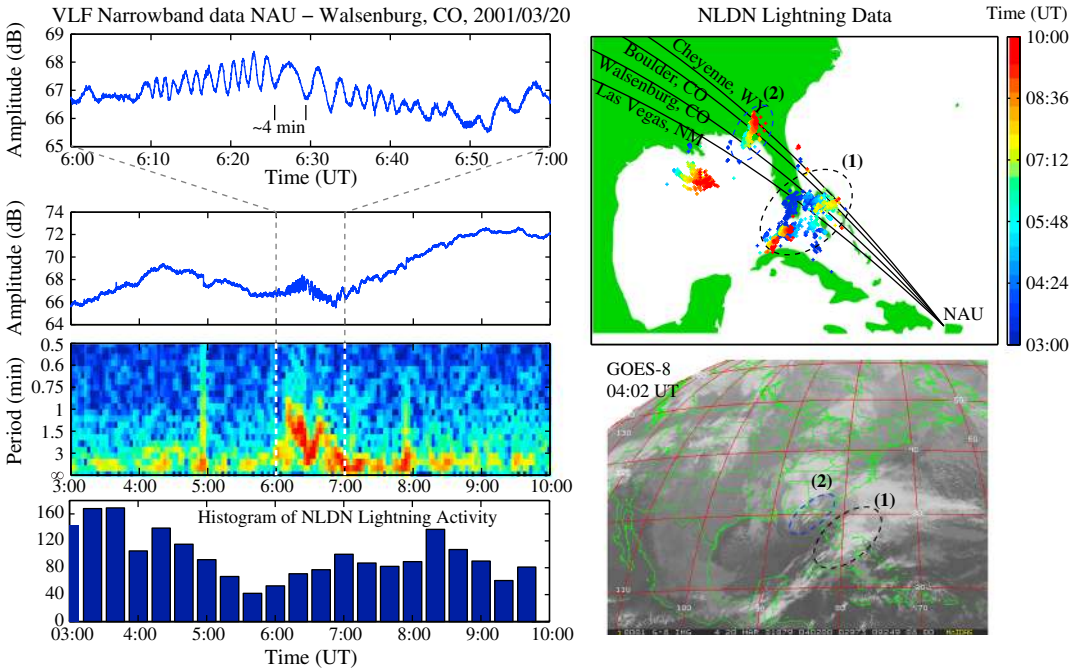

Figure 1. (left, first and second panels) VLF narrowband amplitude data for NAU transmitter (Puerto Rico) measured at Walsenburg, Colorado. (left, third panel) Spectrogram of VLF amplitude variations, demonstrating periodic oscillations in 1–3 min period range. (left, fourth panel) Histogram of NLDN-reported lightning activity during this night. (right, first panel) Map of VLF transmitter paths from NAU in Puerto Rico to HAIL sites and lightning activity from NLDN shown with colors representing UT time. (right, second panel) GOES-8 infrared image at 04:02 UT, showing cloud cover corresponding to thunderstorm activity shown above.

digitization. Amplitude and demodulated phase of known narrowband VLF transmitter signals in the ~20–50 kHz range are recorded at 50 Hz sampling rate, 24 h a day. Further details of the recording systems can be found in *Cohen et al.* [2010].

Figure 1 (right, first panel) shows the locations of the NAU transmitter in Puerto Rico (40.75 kHz, 100 kW radiated power) and selected VLF receivers of the HAIL array. Colored symbols represent lightning discharges reported by the National Lightning Detection Network (NLDN); the color varies with time from blue (3 UT) to red (10 UT), with the color scale shown on the right. Clearly there was significant lightning activity, and likely convective activity, at this time in the Southeastern United States.

Figure 1 (left, first panel) shows narrowband VLF amplitude data recorded at Walsenburg, Colorado. Figure 1 (left, first panel) is simply a zoomed-in view of Figure 1 (left, second panel) from 6 to 7 UT. Figure 1 (left, third panel) is a spectrogram of the filtered amplitude data, after removing the background variation on time scales greater than 12 min, in order to focus on the short-period variations. In the spectrogram, the impulsive features near 5 UT and 8 UT are "early VLF" perturbations caused by transient ionization in the *D* region ionosphere created by the lightning quasi-electrostatic field and/or electromagnetic pulse [e.g., *Inan et al.*, 1995; *Marshall et al.*, 2006].

This event is characterized by short-period fluctuations starting at about 6:08 UT. For the first 17 min these fluctuations appear to be coherent with a period of 1–1.5 min. At 6:25 there are approximately two cycles with a period closer to 3 min, followed by another 22 min of 1–2 min period fluctuations. The fluctuations reach as high as ~1.2 dB peak to peak, comparable to very large early VLF and lightning-induced electron precipitation events [*Marshall et al.*, 2006; *Peter and Inan*, 2007].

Based on the 1–3 min periods of the fluctuations shown in Figures 1 and 2, we argue that these fluctuations are a signature of acoustic waves (AWs) driven by storm activity below, propagating up to, and through the *D* region ionosphere. It is well known that in Earth's middle atmosphere, gravity waves are typically limited to intrinsic periods of ~4 min or longer and acoustic waves to periods of ~5 min or shorter, with some variation with altitude and ambient conditions [e.g., *Snively*, 2013, Figure 1a].

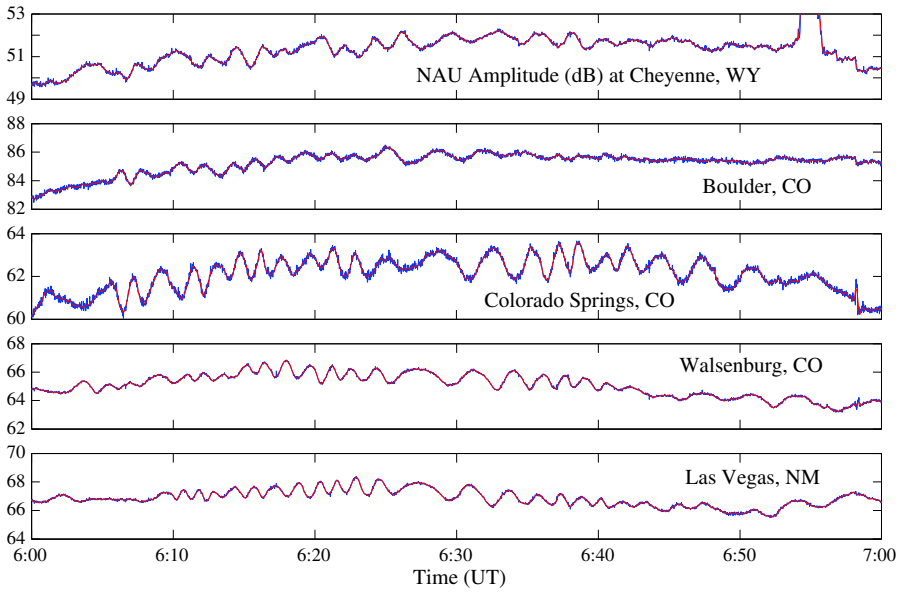

Figure 2. Narrowband VLF data recorded on 20 March 2001, at five HAIL sites, as shown on the map in Figure 1. Blue curves are raw 1 Hz sampled data; red curves are low-pass filtered to reduce noise fluctuations.

Figure 1 (right, second panel) shows satellite imagery from the GOES-8 satellite at 04:02 UT on this day, 2 h before the onset of the oscillations; the next available GOES image was at 07:30 UT, after the oscillations. The lightning activity in Figure 1 can clearly be associated with the two circled storms, a large tropical storm off the southeastern tip of Florida (storm 1) and a small squall line over the Florida panhandle (storm 2).

Figure 2 compares the VLF narrowband data of five VLF receiver sites, namely, Cheyenne, Boulder, Colorado Springs, Walsenburg, and Las Vegas. All five sites observed similar fluctuations; we note that the sites at Walsenburg and Colorado Springs observed the largest fluctuations, and the northernmost site, Cheyenne, observed the smallest fluctuations. While spectrograms from each site show similar features to those in Figure 1, the five sites do observe amplitude fluctuations slightly out of phase with each other. This suggests that a component of the wave was propagating perpendicular to the paths (i.e., north/south) rather than parallel to the paths.

In addition to NAU amplitude data, we have investigated phase data for NAU and amplitude data for the VLF transmitter signals from NAA (Maine), NLK (Washington state), and NPM (Hawaii). Phase data from NAU exhibit some periodic fluctuations similar to the amplitude data, but the SNR is much lower. Amplitude and phase data from NAA, NLK, and NPM do not exhibit fluctuations similar to those shown in Figure 2. These observations suggest that the source of the fluctuations is on the NAU-to-Colorado paths, far from the overlapping NAA paths.

We cannot determine from this data set alone if the perturbation occurred at the location of one or both of the two storms identified in Figure 1 or some other location (i.e., nearer to Puerto Rico). However, if the waves originated from storm 1, they would have to be >210 km wide at the altitude of the ionosphere in the direction perpendicular to the paths in order to appear on all five transmitter paths. If they originated from storm 2, they would have to be >340 km wide at the ionosphere. Either scenario requires a source that is spatially extended and (on average) coherent to produce a sufficiently directive acoustic wave field in the *D* region.

Another feature of the data in Figures 1 and 2 that offers clues to the source is the paucity of very strong "early VLF" events, despite the lightning activity directly below the signal paths. Early VLF events are produced by large lightning discharges, typically those with large charge moments, due to ionization produced by the quasi-electrostatic field directly above the lightning discharge [*Pasko et al.*, 1998]. They do not always appear in the VLF data even when there is an ionospheric disturbance [*Marshall and Inan*, 2010], but they occur more readily when they are near the transmitter [*Haldoupis et al.*, 2010]. There is in fact a single 1.0 dB early VLF event apparent in Figure 1, occurring at 4:56:15 UT on all five paths shown in Figure 2. NLDN did

not report a lightning discharge within 15 s of this event; it is possible that it occurred near the NAU transmitter, beyond NLDN's coverage. However, there are no other early VLF events on 20 March from the NAU transmitter to HAIL. This suggests that the lightning activity shown does not exhibit large charge moments, and thus there is negligible direct electromagnetic coupling to the lower ionosphere.

3. Simulation

We wish to determine the possible AW source configurations that lead to this large-amplitude perturbation on the VLF narrowband signal. To reproduce this perturbation, we use a two-step modeling procedure. First, we use a fluid model of gravity and acoustic wave propagation, with a predefined source input, to calculate the disturbance to the upper atmosphere. Second, we input the atmospheric disturbance to an electromagnetic propagation model of the subionospheric VLF transmitter signal.

3.1. Acoustic and Gravity Wave Model

Acoustic wave propagation is simulated using the model of *Snively* [2013], which may be operated either in Cartesian or cylindrically axisymmetric forms (to investigate radially localized versus horizontally extended sources). It solves the compressible Euler equations with gravity using a finite volume method [e.g., *LeVeque*, 2002] implemented in a modified version of Clawpack (www.clawpack.org). It accounts for viscous and thermal diffusion and source terms arising from geometry [see *Snively*, 2013, section 2.1, and references therein]. A disturbance approximating a series of convective updrafts and downdrafts is imposed as a body force (in units of N/kg ≡ m/s^2):

$$F_s(x,z,t) = \mathcal{F}_0 \exp\left(-\frac{(x-x_0)^2}{2\sigma_x^2} - \frac{(z-z_0)^2}{2\sigma_z^2} - \frac{(t-t_0)^2}{2\sigma_t^2}\right)\cos(\omega t) \tag{1}$$

where σ_x (or σ_r) and σ_z specify the disturbance size in lateral (or radial) and vertical dimensions, σ_t is the disturbance duration modulated by frequency ω, and $\mathcal{F}_0$ is the amplitude. The altitude z_0 of the source is held constant at 12 km and the vertical size is $\sigma_z = 3$ km. We investigate variations in the lateral (or radial) size σ_x (or σ_r) from 3 km to 150 km, and amplitude $\mathcal{F}_0$ from 0.01 to 0.2 N/kg.

In addition to source parameters, we vary the background ionosphere profile to investigate its effects on the perturbation amplitude. The ionospheric profile choice has the strongest effects on the VLF transmitter electromagnetic (EM) wave propagation and also affects the shape and altitude of the disturbance produced in the AGW model. We discuss the choices of ionospheric profile in the next section.

3.2. EM Propagation Model

To simulate the propagation of the VLF transmitter signal, we use a segmented long-path finite-difference frequency domain (FDFD) model of subionospheric VLF propagation [*Chevalier and Inan*, 2006]. This model allows for arbitrarily specified electron density and collision frequency in 2-D (altitude range, cylindrical coordinates) [*Marshall and Inan*, 2010]. We begin with an ionospheric electron density profile specified either by the International Reference Ionosphere (IRI) model [*Bilitza and Reinisch*, 2008] or the *Wait and Spies* [1964] (WS) model where the electron density n_e in cubic centimeters at altitude h is given by

$$n_e(h) = 1.43 \times 10^7 \exp(-0.15h') \times \exp\left[(\beta - 0.15)(h - h')\right] \tag{2}$$

where h' is a reference altitude, typically 83–87 km, and β is a "sharpness" parameter, which is typically varied between 0.5 and 0.9. Note that β is effectively the inverse of the ionosphere scale height; higher β corresponds to a smaller scale height, or sharper profile near h'. We also use an MSIS-E-90 atmospheric density profile [*Hedin*, 1991], from which the collision frequency is specified by $\nu_e = (q_e/m_e)/\mu_e$, with the electron mobility $\mu_e = 1.4856N_0/N$, and N is the neutral density as a function of altitude [e.g., *Pasko et al.*, 1997]. We use the same ionosphere and atmosphere profiles in the propagation mode and the fluid model in each particular case. We input the disturbance produced by the fluid model at the approximate location along the great-circle-path of one of the two thunderstorms (over either South Florida or the Florida panhandle). The model takes into account real ground conductivity and magnetic field direction and amplitude for the specified path.

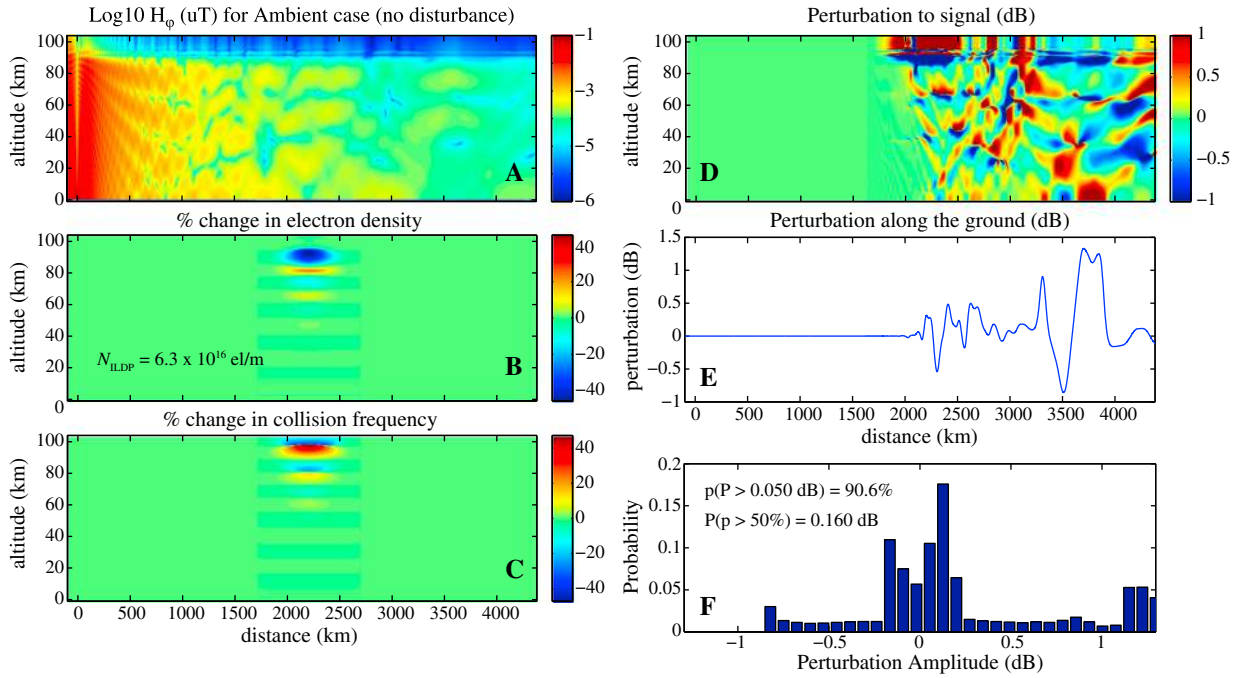

Figure 3. Results from example simulation. (a) Amplitude of H_ϕ component on log scale in altitude range space. (b and c) Percent change in electron density and collision frequency, as determined by AGW model. Δv_e is computed from the output Δn_d, the change in neutral density. (d) The perturbed signal in 2-D space, taken as the difference (in dB) between the ambient and disturbed fields. (e) Perturbation sampled along the ground. This is what a VLF receiver measured as ΔA. (f) Histogram of measured perturbation if a receiver is randomly placed in the last 1000 km of the simulation space.

3.3. Simulation Results

Figure 3 shows example simulation results from this model. This case uses a WS ionosphere model with $h' = 87$ km and $\beta = 0.9$, the highest and sharpest ionosphere profile considered. The disturbance has an amplitude of $\mathcal{F}_0 = 0.05$ N/kg, and a size $\sigma_x = 150$ km, located over the Florida panhandle (storm 2). As with all simulation cases, ω corresponds to a period of 60 s, $t_0 = 360$ s, and $\sigma_t = 60$ s (i.e., the source includes only two to three cycles at the source period). Figure 3a shows the 2-D H_ϕ component (i.e., perpendicular to the page) versus altitude and along the transmitter path for the "ambient" case. Typical of these simulations, one can immediately see mode interference; reflection from the base of the ionosphere at 85 km; and amplitude decay with distance, primarily due to spreading in the Earth-ionosphere waveguide. Figures 3b and 3c show the electron density and collision frequency disturbances calculated from the fluid model as a percent change from the ambient. The FDFD model is then rerun with the modified ionosphere, and the difference in decibel amplitudes is shown in Figure 3d. This perturbation exceeds 5 dB at many locations in the 2-D space, due to shifting of the interference nulls. However, along the ground (Figure 3e), the perturbation is somewhat more regular and rarely exceeds 1 dB.

Figure 3e shows that a VLF receiver located at some distance x along the x axis would measure the perturbation shown at that location. In our experimental setup, the VLF receiver is at the far right end of the path (4500 km from NAU). The amplitude at any given location is highly sensitive to the mode interference in the waveguide, which is sensitive to the poorly known electron density profile, which varies considerably both in time and space [e.g., *Marshall and Inan*, 2010]; as such, the end point of this figure is a poor predictor of the actual measured amplitude. To make a statistical prediction of the measured perturbation, we calculate a distribution of perturbation amplitudes in the last 1500 km of the path at 500 m increments. We then calculate the probability that the measured perturbation at a given location is greater than 0.05 dB (roughly the threshold of detectability in the data) and the perturbation amplitude for which the probability exceeds 50% (i.e., the median). In the case shown, there is a 90.6% chance that the perturbation measured at any given point will exceed 0.05 dB, and the 50% probability threshold is 0.16 dB. For comparison, the measured amplitude perturbation in Figures 1 and 2 reaches ~0.6 dB.

Table 1. Summary of Simulations[a]

Source Type	Source $\mathcal{F}_0$	Source Size (in x or r)	Ionosphere	h', β	VLF Reflection Height	N_{ILDP} (10^{16} e$^-$/m)	$P > 50\%$ (dB)
"First test"	0.1	50 km	WS	85, 0.9	85 km	~0.4	~0.01
"Realistic ionosphere"	0.1	50 km	IRI-like		85.3 km	~0.16	~0.01
"h-beta tests"	0.1	50 km	WS	83–87, 0.5–0.9	83–87 km	~0.6–6	0.02–0.5
"Corrugated n_e"	0.05	3 km	WS	87, 0.7	87 km	~0.1–0.2	~0.01
"Large source size"	0.05	150 km	WS	87, 0.9	87 km	~2–3	0.05–0.18
"Two sources, IRI"	0.02, 0.04	150, 50 km	IRI		82 km	~1–2	0.01–0.06
"Two sources, WS"	0.02, 0.04	150, 50 km	WS	87, 0.9	87 km	~0.6–2	0.03–0.1

[a]The VLF reflection height is derived from the electron and neutral density profiles. The last two columns are measured from the EM propagation simulations.

We aim to determine the source parameters (amplitude and size) and ionospheric conditions under which the measured perturbation can be reproduced. For this purpose, we have run a variety of simulations with different source amplitudes and sizes as described in section 3.1. We vary the ionosphere by using either an IRI ionosphere or a WS profile, with h' varied from 83 to 87 km, and β varied from 0.5 to 0.9. All simulations use the MSIS-E-90 atmospheric profile for the time and location of storm 1. The ionosphere and atmosphere profiles lead directly to an estimate of the VLF reflection height h_R, which is the altitude at which $\omega_p^2 = \nu_e\omega$ [*Ratcliffe*, 1959]; h_R is not necessarily the same height as h', depending on the MSIS-E-90 profile, but in our simulations $|h_R - h'| \leq 1$ km. Table 1 summarizes the simulation runs and output parameters. The "two sources" cases separately simulate a 150 km, cylindrically symmetric source near South Florida or a 50 km wide Cartesian source over the Florida panhandle at the locations of storms 1 and 2, respectively.

We follow the method of *Peter and Inan* [2007] to compare the density disturbance to the measured perturbation amplitude. Since the VLF wave is most sensitive to Δn_e and $\Delta\nu_e$ in a narrow altitude range around h_R, we define the "integrated line density perturbation" N_{ILDP} as the change in electron density integrated along the transmitter-receiver path, through an altitude range $\Delta h = 6$ km centered around h_R:

$$N_{ILDP} = \int_{l_{xmtr}}^{l_{rcvr}} \int_{h_R-\Delta h/2}^{h_R+\Delta h/2} \Delta n_e(l,h)\, dh\, dl \tag{3}$$

This is a modest change from the method of *Peter and Inan* [2007], who integrated strictly from 80 to 85 km altitude, irrespective of the ionospheric conditions; this modified measurement looks specifically at the density change around the VLF reflection height, where the wave-ionosphere interaction is strongest.

Figure 4 shows N_{ILDP} for two particular cases from the "two sources" set of runs. Both of these cases use the WS ionosphere profile, with $h' = 87$ km and $\beta = 0.9$. As described earlier, the "panhandle source" case places a 50 km wide 2-D Cartesian source at the location of storm 2, on the Florida panhandle, with an amplitude of $\mathcal{F}_0 = 0.04$ N/kg. The "South Florida" case places a 150 km wide, cylindrically symmetric source at the location of storm 1, near the tip of Florida, with an amplitude of $\mathcal{F}_0 = 0.02$ N/kg. We observe that these two cases yield maximum N_{ILDP} of ~1.5×10^{16} el/m; the smaller, although larger-amplitude, panhandle source provides a smaller N_{ILDP} due to the reduced spatial extent of the disturbance along the VLF path.

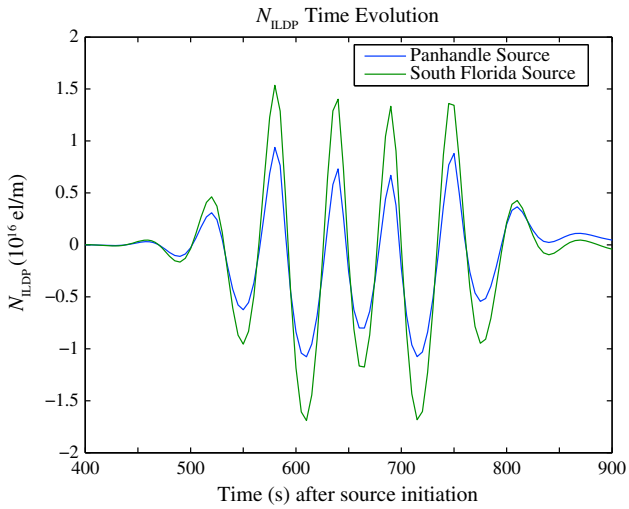

Figure 4. Integrated line density perturbation (N_{ILDP}) for two source cases; see the text for description of the source inputs.

It is notable that, in both cases, the density fluctuations exhibit

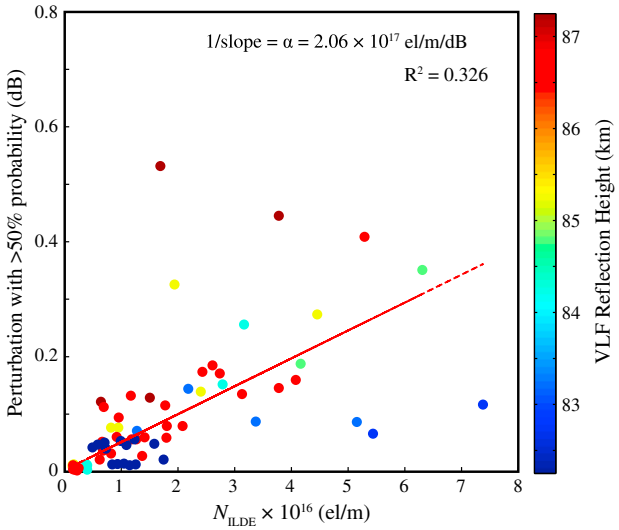

Figure 5. Simulation statistics. The N_{ILDP} can be measured from the AGW simulation outputs; the perturbation amplitude is taken from the EM simulations. Results show a reasonable correlation between N_{ILDP} and ΔA but show a further dependence on other parameters such as h_R, the VLF reflection height.

approximately five cycles at the source period, while the source itself had only two to three cycles. This arises due to the ground reflection of downward acoustic waves launched simultaneously by the tropospheric sources, leading to a second packet of coherent waves that follows the initial packet.

Figure 5 shows the results of a large number of simulations, comparing N_{ILDP} and ΔA, the perturbation amplitude measured by the VLF receiver. The absolute value of the amplitude perturbation is taken here for comparison. It is found that positive N_{ILDP} values may produce either positive or negative ΔA perturbations to the VLF signal, depending on the location of the receiver (perhaps contributing to the observed phase differences between receivers). The scattered points are color coded by the VLF reflection height for that simulation. We observe that a reasonable correlation exists between these parameters. The inverse slope, corresponding to α_{ILDP} in *Peter and Inan* [2007], is 2.06×10^{16} el/m/dB; for comparison, *Peter and Inan* [2007] found $\alpha_{\mathrm{ILDP}} = 5.1 \times 10^{16}$ el/m/dB, albeit for only two cases of lightning-induced electron precipitation. We have similarly tested an "integrated collision frequency perturbation" parameter, but it does not correlate as strongly with ΔA.

These results show that to produce a 0.5 dB amplitude perturbation, we require N_{ILDP} of $\sim 10^{17}$ el/m. Only a handful of our simulations produce disturbances of this magnitude, but it is within the range that physically reasonable simulations can reproduce (resulting in acoustic wave disturbances at ~100 Pa within the source). In general, the largest perturbations are found for large sources (both in amplitude and size) and with ionospheric profiles that are high (large h_R) and sharp (large β). Intuitively, higher h_R means the EM wave can probe to a higher altitude, where the AW also has higher amplitude, due to exponential growth with altitude. Higher β is less intuitive but may imply that the EM wave is less attenuated in the altitude range just below the reflection height, so more of the wave reaches h_R and just above.

4. Discussion and Conclusions

We have presented the first observation of acoustic waves observed in VLF subionospheric remote sensing. We hypothesize that these waves are launched by thunderstorm/convective activity in one of two thunderstorms occurring along the VLF signal path. We model the acoustic wave propagation and disturbance of the overlying ionosphere and the VLF transmitter signal propagation in the Earth-ionosphere waveguide and estimate the source amplitude and size necessary to produce the observed signature. We find that very large sources (producing wave perturbations to *D* region electron density tens of percent, spanning >100 km radially) are required to produce the observed perturbation of 0.5 dB. We further find that the perturbation is larger for higher h_R and larger β (i.e., sharper ionospheric profiles).

The correlation between N_{ILDP} and ΔA also suggests that waves able to significantly perturb the N_{ILDP} will be most readily observable. This provides an observational "filtering" mechanism; acoustic waves that are horizontally coherent in the *D* region, due to high source directivity, appear most likely to produce strong N_{ILDP} perturbations and also produce strong ΔA perturbations. Less directive sources that produce "corrugated" wave fields with many alternating wavelengths (in the radial direction) through the *D* region yield small N_{ILDP} perturbations on average. This also suggests a filtering effect for gravity waves; their horizontally periodic structure may tend to produce weak N_{ILDP} perturbations for waves propagating along the direction of the VLF signal, due to integrated cancelation through alternating phase fronts. Gravity waves propagating

perpendicular to the VLF path, with sufficiently long horizontal wavelengths and extents, may produce N_{ILDP} perturbations more effectively. These selective filtering effects will be investigated in future work; however, we suggest that they may provide a mechanism for coherent signatures to arise despite the relatively broad wave spectra anticipated above realistic convective sources.

Thus, under the hypothesis that the perturbation is caused by convective activity in the troposphere, a very large wave source is required. We cannot definitely correlate this observation to convective AW activity, but we can rule out a few other possibilities. This disturbance is unlikely to have been caused by earthquake activity [e.g., *Matsumura et al.*, 2011]; no earthquakes were recorded in North America on this day by the US Geological Survey. It is also unlikely to be caused by propagation of waves from higher latitudes (i.e., auroral forcing), because no similar activity was observed on the NAA-to-HAIL paths north of the NAU-to-HAIL paths. However, the geomagnetic *A* index on this day was 105 at high latitudes and 27 at midlatitudes, as documented on the NOAA Space Environment Center website. A moderate-to-strong geomagnetic storm occurred from 00:00 to 18:00 UT. The high-latitude *A* index value was the highest for all of 2001. It is possible that this geomagnetic disturbance is alternately responsible for the observed perturbation or perhaps responsible for modifying the *D* region ionosphere to make observation of the convectively driven AW more favorable. There is also the possibility that the acoustic waves were generated by a meteor entering the atmosphere, similar to *Hecht et al.* [2002]. However, the observations in that paper occurred at the time of a meteor shower, while the present event does not; and the *Hecht et al.* [2002] event had no convective activity nearby with which to correlate, while the present event clearly does.

An alternative explanation for the large observed amplitude perturbation is revealed in the 3500–4000 km range of Figure 3. In this region the AW perturbation to the VLF wave reaches 1 dB over a wide area, but the average disturbance that is measurable from 2500 to 4000 km is only 0.16 dB due to the regions of smaller perturbation. It is possible that the ionospheric conditions at the time of this event enabled a fortuitously large perturbation to be measured just at the receiver, i.e., that the range was near optimal for detecting this disturbance. If that is the case, we expect this event to be an unusual event. Statistical searches have uncovered other similar events with smaller amplitudes; however, a detailed statistical study of AW event occurrence in VLF-SRS is ongoing and left for future work.

Acknowledgments

R.A. Marshall was supported by NSF CEDAR/GEM Postdoctoral Fellowship AGS-1027070 and NSF CEDAR grant AGS-1243176. Research by J.B. Snively was supported by NSF CAREER grant AGS-1151746 to Embry-Riddle Aeronautical University. The VLF narrowband data set and simulation outputs are available upon request from the authors.

References

Bilitza, D., and B. Reinisch (2008), International reference ionosphere 2007: Improvements and new parameters, *J. Adv. Space Res.*, *42*(4), 599–609, doi:10.1016/j.asr.2007.07.048.

Chevalier, M. W., and U. S. Inan (2006), A technique for efficiently modeling long-path propagation for use in both FDFD and FDTD, *IEEE Antennas Wirel. Propag. Lett.*, *5*, 525–528.

Cohen, M. B., U. S. Inan, and E. W. Paschal (2010), Sensitive broadband ELF/VLF radio reception with the AWESOME instrument, *IEEE Trans. Geosci. Remote Sens.*, *48*, 3–17.

Fritts, D. C., and M. J. Alexander (2003), Gravity wave dynamics and effects in the middle atmosphere, *Rev. Geophys.*, *41*(1), 1003, doi:10.1029/2001RG000106.

Galvan, D. A., A. Komjathy, M. P. Hickey, P. Stephens, J. Snively, Y. T. Song, M. D. Butala, and A. J. Mannucci (2012), Ionospheric signatures of Tohoku-Oki tsunami of March 11, 2011: Model comparisons near the epicenter, *Radio Sci.*, *47*, RS4003, doi:10.1029/2012RS005023.

Garcia, R. F., S. Bruinsma, P. Lognonné, E. Doornbos, and F. Cachoux (2013), GOCE: The first seismometer in orbit around the earth, *Geophys. Res. Lett.*, *40*, 1015–1020, doi:10.1002/grl.50205.

Georges, T. M. (1973), Infrasound from convective storms: Examining the evidence, *Rev. Geophys. Space Phys.*, *11*(3), 571–594.

Haldoupis, C., N. Amvrosiadi, B. R. T. Cotts, O. A. van der Velde, O. Chanrion, and T. Neubert (2010), More evidence for a one-to-one correlation between sprites and early VLF perturbations, *J. Geophys. Res.*, *115*, A07304, doi:10.1029/2009JA015165.

Hecht, J. H., R. L. Walterscheid, M. P. Hickey, R. J. Rudy, and A. Z. Liu (2002), An observation of a fast external atmospheric acoustic-gravity an observation of a fast external atmospheric acoustic-gravity wave, *J. Geophys. Res.*, *107*(D20), 4444, doi:10.1029/2001JD001438.

Hedin, A. E. (1991), Extension of the MSIS thermospheric model into the middle and lower atmosphere, *J. Geophys. Res.*, *96*(A2), 1159–1172, doi:10.1029/90JA02125.

Inan, U. S., T. F. Bell, V. P. Pasko, D. D. Sentman, E. M. Wescott, and W. A. Lyons (1995), VLF signatures of ionospheric disturbances associated with sprites, *Geophys. Res. Lett.*, *22*(24), 3461–3464.

Johnson, M. P., U. S. Inan, S. J. Lev-Tov, and T. F. Bell (1999), Scattering pattern of lightning-induced ionospheric disturbances associated with early/fast VLF events, *Geophys. Res. Lett.*, *26*(15), 2363–2366.

Laštovička, J. (2006), Forcing of the ionosphere by waves from below, *J. Atmos. Sol. Terr. Phys.*, *68*, 479–497.

LeVeque, R. J. (2002), *Finite Volume Methods for Hyperbolic Problems*, Cambridge Univ. Press, Cambridge, U. K.

Marshall, R. A., and U. S. Inan (2010), Two-dimensional frequency-domain modeling of lightning-induced perturbations to VLF transmitter signals, *J. Geophys. Res.*, *115*, A00E29, doi:10.1029/2009JA014761.

Marshall, R. A., U. S. Inan, and W. A. Lyons (2006), On the association of early/fast very low frequency perturbations with sprites and rare examples of VLF backscatter, *J. Geophys. Res.*, *111*, D19108, doi:10.1029/2006JD007219.

Matsumura, M., A. Saito, T. Iyemori, H. Shinagawa, T. Tsugawa, Y. Otsuka, M. Nishioka, and C. H. Chen (2011), Numerical simulations of atmospheric waves excited by the 2011 off the Pacific coast of Tohoku earthquake, *Earth, Planets, Space*, *63*(7), 885–889, doi:10.5047/eps.2011.07.015.

Pasko, V. P., U. S. Inan, T. F. Bell, and Y. N. Taranenko (1997), Sprites produced by quasi-electrostatic heating and ionization in the lower ionosphere, *J. Geophys. Res.*, *102*(A3), 4529–4561.

Pasko, V. P., U. S. Inan, and T. F. Bell (1998), Ionospheric effects due to electrostatic thundercloud fields, *J. Atmos. Sol. Terr. Phys.*, *60*, 863–870.

Peter, W. B., and U. S. Inan (2005), Electron precipitation events driven by lightning in hurricanes, *J. Geophys. Res.*, *110*, A05305, doi:10.1029/2004JA010899.

Peter, W. B., and U. S. Inan (2007), A quantitative comparison of lightning-induced electron precipitation and VLF signal perturbations, *J. Geophys. Res.*, *112*, A12212, doi:10.1029/2006JA012165.

Pilger, C., C. Schmidt, and M. Bittner (2013), Statistical analysis of infrasound signatures in airlgow observations: Indications for acoustic resonance, *J. Atmos. Sol. Terr. Phys.*, *93*, 70–79.

Ratcliffe, J. A. (1959), *The Magneto-Ionic Theory and its Applications to the Ionosphere*, Cambridge Univ. Press, Cambridge.

Snively, J. B. (2013), Mesospheric hydroxyl airglow signatures of acoustic and gravity waves generated by transient tropospheric forcing, *Geophys. Res. Lett.*, *40*, 4533–4537, doi:10.1002/grl.50886.

Wait, J. R., and K. P. Spies (1964), Characteristics of the Earth-ionosphere waveguide for VLF radio waves, *Tech. Note 300*, Natl. Bur. of Stand., Boulder, Colo.